Met. Mater. Int., Vol. 18, No. 4 (2012), pp. 607~612
doi: 10.1007/s12540-012-4006-y

Corrosion Behaviors of Coatings Fabricated Using Bulk Metallic Glass Powders with the Composition of $Fe_{68.5}C_{7.1}Si_{3.3}B_{5.5}P_{8.7}Cr_{2.3}Mo_{2.5}Al_{2.0}$

S. L. Wang[1], H. X. Li[2], S. Y. Hwang[3], S. D. Choi[3], and S. Yi[4,*]

[1]School of Aeronautical Manufacturing Engineering, Nanchang Hangkong University, Nanchang 330063, China
[2]State Key Laboratory for Advanced Metals and Materials, University of Science and Technology Beijing, Beijing, 100083, China
[3]Research Institute of Industrial Science and Technology, Pohang 790-600, Korea
[4]Department of Materials Science and Metallurgy, Kyungpook National University, Daegu 702-701, Korea

(received date: 8 July 2010 / accepted date: 18 August 2010)

Two different types of coatings were prepared, by a high velocity oxy-fuel spraying method and a laser spraying method, respectively, using bulk metallic glass powders with the nominal composition of $Fe_{68.5}C_{7.1}Si_{3.3}B_{5.5}P_{8.7}Cr_{2.3}Mo_{2.5}Al_{2.0}$. The corrosion behaviors of the two coatings in 1M HCl, H_2SO_4, NaCl and NaOH solutions were investigated based upon the microstructural differences originating from the different coating methods. The amorphous coating layer formed by the high velocity oxy-fuel spraying method exhibited higher, excellent corrosion resistance in the 1M HCl solution. The coating layer formed by the laser spraying method exhibited a high pitting tendency attributed to the dendritic microstructure with various borides and carbides. Due to a great number of pores, the HVOF coating exhibits slightly lower corrosion resistance than the LS coating in alkaline solution.

Key words: amorphous materials, coating, corrosion, surface modification, plasma deposition/spray

1. INTRODUCTION

Fe-based bulk metallic glasses (Fe-BMGs) are attractive for practical applications due to their high strength, good soft-magnetic properties and excellent corrosion resistances [1-3]. However, the extremely poor tensile ductility of Fe-BMG is a critical drawback for extensive application as bulk structural materials. On the other side, the Fe-BMGs with high glass forming ability (GFA) can be applied in practice as anti-wear or anti-corrosive coating materials for metallic components [4,5]. That is, amorphous or nanostructured coating layers with low wear loss or high corrosion resistance can be fabricated through various coating methods using Fe-BMG powders. From previous works [6,7], excellent corrosion resistance of some Fe-BMGs has been reported. However, due to the relatively low GFA of Fe-BMGs, the corrosion behaviors of an amorphous coating layer fabricated using Fe-BMGs powders have not been extensively studied to date. Although some Fe-BMGs have a range of GFA high enough to form amorphous coating layers, those Fe-BMGs include expensive and reactive alloying elements such as Yittrium or Erbium, which limit materials processing conditions and raise unit cost for the coating process [8,9]. Therefore, for practical applications of Fe-BMGs as coating materials, the Fe-BMGs need to have high GFA as well as cost-effectiveness for processing. Along the line to develop Fe-BMGs with high GFA using industrial raw materials and commercial materials processing, Fe-BMGs have been developed using cast iron, industrial ferro-alloys and commercial grade elements [10,11]. In this study, using atomized powders of the Fe-BMG $Fe_{68.5}C_{7.1}Si_{3.3}B_{5.5}P_{8.7}Cr_{2.3}Mo_{2.5}Al_{2.0}$, two different types of microstructure coatings have been produced, by a high velocity oxy-fuel spraying (HVOF) method and a laser spraying (LS) method, respectively. Corrosion behaviors of the coatings were investigated to understand the microstructural effects on corrosion resistance in various solutions.

2. EXPERIMENTAL PROCEDURES

Fe-BMG powders with the nominal composition of $Fe_{68.5}C_{7.1}Si_{3.3}B_{5.5}P_{8.7}Cr_{2.3}Mo_{2.5}Al_{2.0}$ were prepared through a commercial gas atomization technique using the industrial

*Corresponding author: yish@knu.ac.kr

Table 1. Chemical compositions (wt%) of industrial raw materials used in this study

Materials	C	Si	B	P	Cr	Mn	Ti	Al	Ni	Ca	O	N	S
Cast iron	4.28	0.46	---	0.20	---	0.20	0.03	---	0.09	---	---	---	0.04
Fe-P	0.02	0.01	---	26.28	---	0.69	0.35	---	---	0.01	---	---	0.01
Fe-B	0.17	0.65	19.75	0.04	---	0.21	---	0.05	---	---	0.02	0.01	---
Fe-Cr	1.43	0.33	---	0.02	55.49	---	---	---	---	---	0.24	0.01	---

*Commercial pure elements (Al, Si, Mo) > 95%

Table 2. Experimental conditions for the HVOF coating process

Spray parameters	Conditions
Oxygen flow rate (SCFH)	1975
Fuel flow rate (GPH)	4.2
Powder feeding rate (g/min)	76
Fuel type	Kerosene
Spray distance (mm)	300

raw materials listed in Table 1. For the coating process, a low alloyed carbon steel plate with a dimension of 60 × 35 × 7 mm were degreased in acetone and sandblasted to secure good bonding between the coating layer and the substrate. The coatings were produced using a high velocity oxy-fuel spraying (HVOF, JP-5000) with the spraying experimental condition given in Table 2. Laser spraying was carried out with a 2 kW fiber laser while powders were sprayed with a coaxial spraying gun. The spraying gun velocity was 500 mm/min, and the gun distance was 100 mm.

The crystalline phases in the coatings were identified from x-ray diffraction (XRD, Philip X'Pert diffractometer) with Cu radiation (Cu-Kα, $\lambda = 0.1541$ nm). The microhardness of the coating layers was determined using a Vickers microhardness tester (HMW-2000, Shimadzu) with a load of 500 g for 10 seconds. Electrochemical measurements were conducted with an EG&G Pinceton Applied Research PARSTAT 2273 potentiostat with EG&G powersuit software (Princeton Applied Research, Oak, TN). The electrochemical cell contained a central inlet for the working electrode, a Luggin probe connected with a saturated calomel reference electrode (KCl), and graphite counter electrode. The potentiodynamic polarization curves were measured with a 50 mV/min potential sweep rate in 1M HCl, H_2SO_4, NaCl and NaOH solutions, respectively, open to air at 293K after immersion for 30 mins.

3. RESULTS

3.1. Characterization of coating layers

A great number of pores and spherical powders can be observed on the HVOF coating surface, while only a few small pores can be seen on the LS coating surface, from the SEM images shown in Fig. 1(a) and 2(a). The cross-section view of the LS coating layer shows a fairly dense coating layer well-bonded on the substrate, unlike the case of the

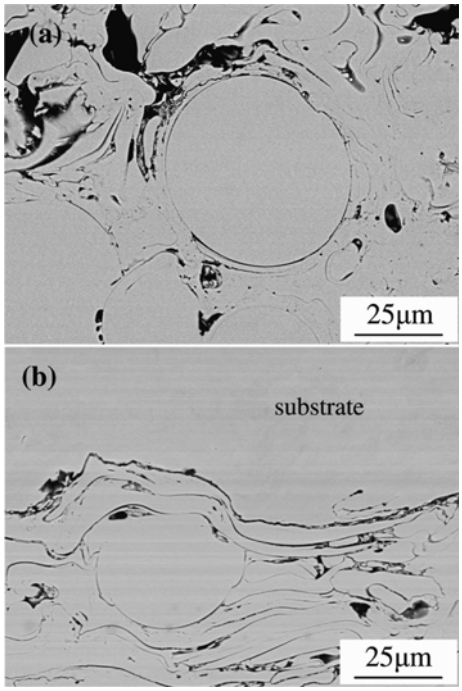

Fig. 1. SEM micrographs of HVOF coating: (a) top surface, (b) cross sectional plane.

HVOF coating layer (Fig. 1(b) and 2(b)). Since a large amount of heat per unit area was imposed during the LS coating process, the powders, as well as the surface of the substrate, were completely melted and then solidified, yielding the dense coating layer with dendritic microstructure. The crystalline phases in the LS coating layer can be identified as α-Fe, Fe_3B, Fe_3P and Fe_3C phases from the XRD pattern shown in Fig. 3(a). The XRD pattern from the HVOF coating layer, however, which is only a halo pattern typical for an amorphous phase, can be obtained as shown in Fig. 3(b). Figure 4 presents the microhardness profiles as a function of cross sectional depth from the surface for the LS and the HVOF coating layers, respectively. The microhardness value of the HVOF coating layer was measured to be ~350 Hv, while a high value of ~730 Hv was obtained for the LS coating layer. It is well known that bulk metallic glass generally exhibits a high microhardness approaching 1250 Hv [12]. The relatively low microhardness value of the HVOF coating layer, which has an amorphous structure, is due to the existence of a great number of pores, as shown in Fig.

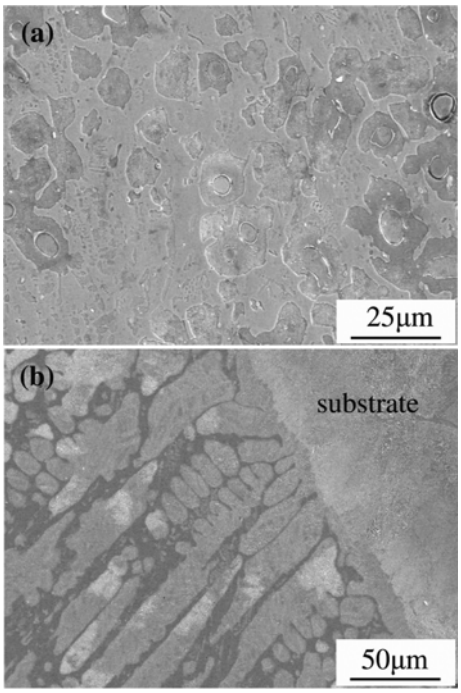

Fig. 2. SEM micrographs of LS coating: (a) top surface, (b) cross sectional plane.

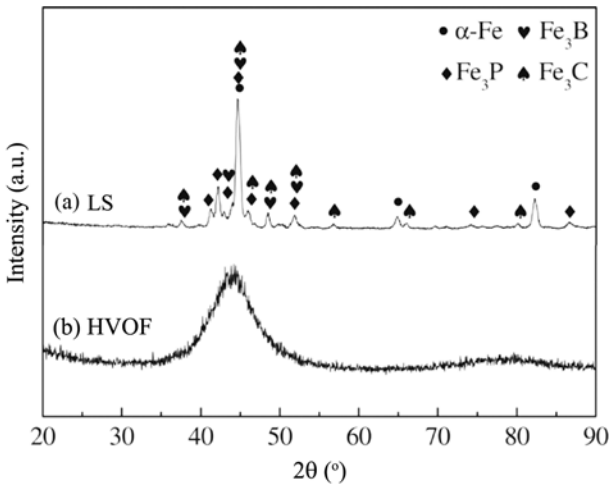

Fig. 3. XRD patterns of LS (a) and HVOF coating (b).

1(a) and (b). The high microhardness of the LS coating can be attributed to the presence of complex carbide and boride phases dispersed in the fine ferritic grains [4,5].

3.2. Corrosion behaviors of coating layers

The anodic polarization curves of the HVOF and LS coatings were estimated in 1M HCl, H_2SO_4, NaCl and NaOH solutions, respectively, with a scanning velocity of 50 mV/min at room temperature. Figure 5 shows the polarization curves measured in acidic solutions. It can be observed that the HVOF and LS coatings are spontaneously passivated with

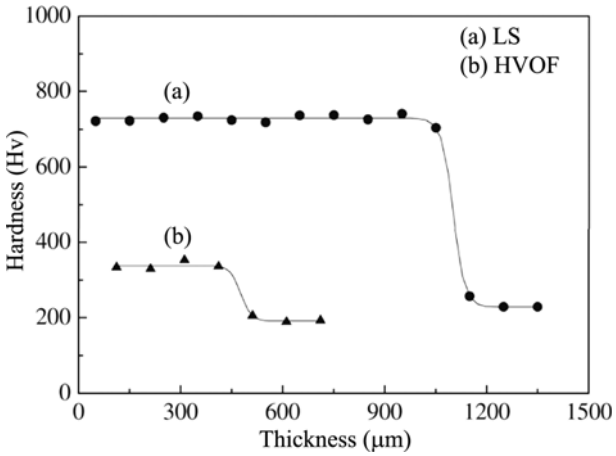

Fig. 4. Microhardness profile with depth along the cross sectional plane perpendicular to the top surface of LS (a) and HVOF coating (b).

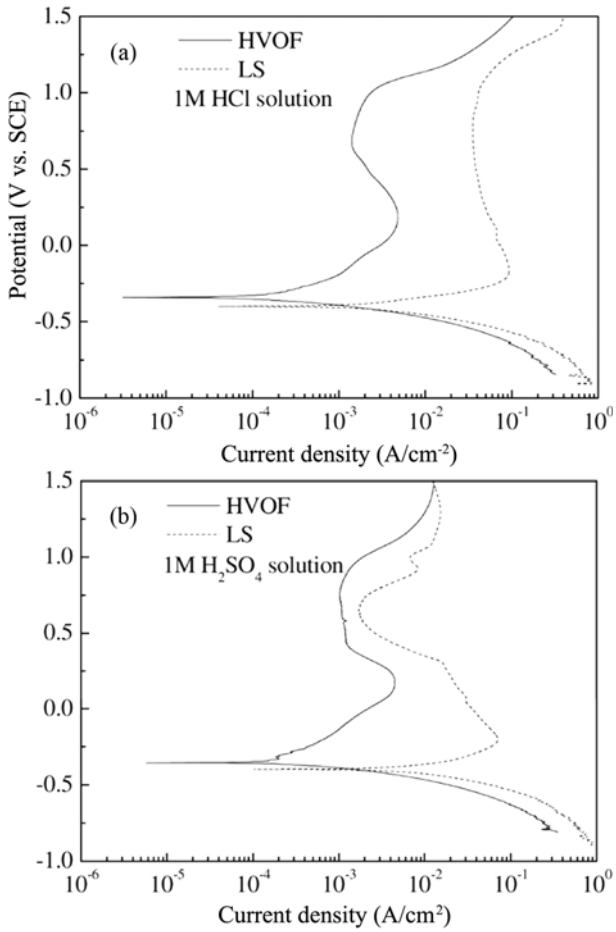

Fig. 5. Potentiodynamic polarization curves in various solutions: (a) 1M HCl, (b) 1M H_2SO_4.

low passive current density and wide passive region. The passive current density (I_{pass}) of the HVOF coating is 4.8 and 4.5 mA/cm^2 in the HCl and the H_2SO_4 solutions, respectively, while those for the LS coating are 94.1 mA/cm^2 and

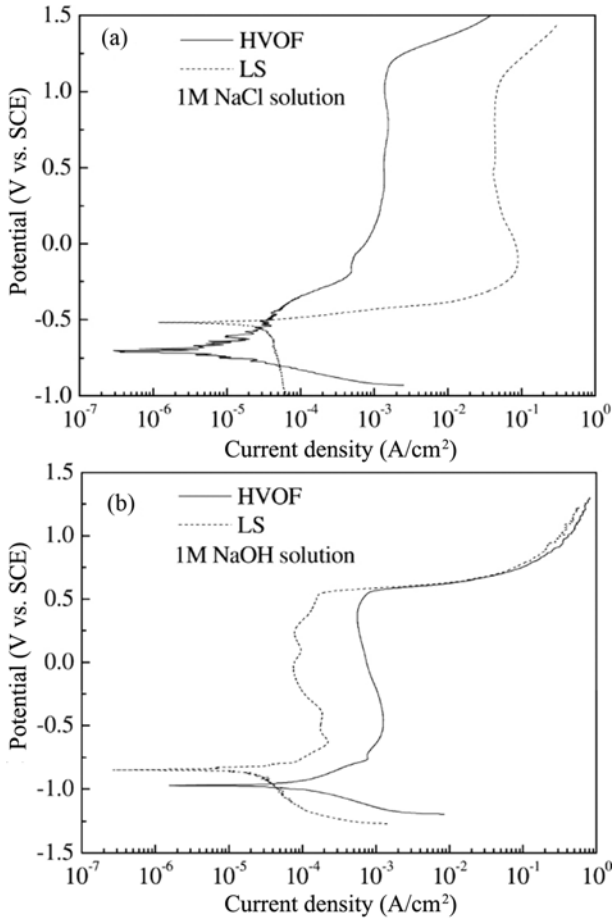

Fig. 6. Potentiodynamic polarization curves in various solutions: (a) 1M NaCl, (b) 1M NaOH.

70.0 mA/cm^2 in the HCl and the H_2SO_4 solutions, respectively. The LS coating presents a more negative corrosion potential (E_{corr}) and higher corrosion current density (I_{corr}) than that of HVOF coating in acidic solutions. The opposite tendency of the polarization curves can be obtained from the measurements in the alkaline solutions (Fig. 6). That is, in the 1M NaOH solution, the LS coating exhibited more positive corrosion potential and lower corrosion current density and passive current density than the HVOF coating. Meanwhile, the LS coating showed more positive E_{corr}, larger I_{corr} and I_{pass} than the HVOF coating in the 1M NaCl solution. The corrosion potential (E_{corr}) and corrosion current density (I_{corr}) in each solution are summarized in Table 3. It can be observed in Table 3 that the E_{corr} for the HVOF coating and LS coating in acidic solution is more positive than in the alkaline solution, respectively. The similar tendency in corrosion potential has also been reported for the Fe-Cr-Mo-Er-C-B bulk metallic glass [13] and Fe-based ferromagnetic bulk glassy alloys [14].

The polarization resistance R_p, an indirect measurement of corrosion resistance, is calculated according to equation (1) [15]:

Table 3. Results of the potentiodynamic polarization and the polarization resistance

	Soultion	HCl	H_2SO_4	NaCl	NaOH
HVOF	V_{corr} (-mV)	341	354	707	972
	I_{corr} (μa/cm^2)	131.9	258.8	2.3	37.7
	R_p (Ωcm^2)	130.4	88.4	6885.2	434.4
LS	V_{corr} (-mV)	397	400	519	848
	I_{corr} (μa/cm^2)	2092.7	6507.8	32.1	13.8
	R_p (Ωcm^2)	8.8	3.4	722.5	1642.4

$$R_p = \beta_\alpha\beta_c/[2.3I_{corr}(\beta_\alpha+\beta_c)] \quad (1)$$

where β_α and β_c are the slope of tangents drawn on the respective anodic and cathodic polarization plots. The results of the polarization resistance listed in Table 3 indicate that the HVOF coating presents higher, excellent corrosion resistance in the acidic solution.

The potentiostatic polarizations were measured in 1M HCl and NaOH solutions, respectively. The observed current density vs. passivation time is plotted in Fig. 7. The applied potential of 0.7V and 0.35V, corresponding to the passive region in the HCl and the NaOH solutions, respectively,

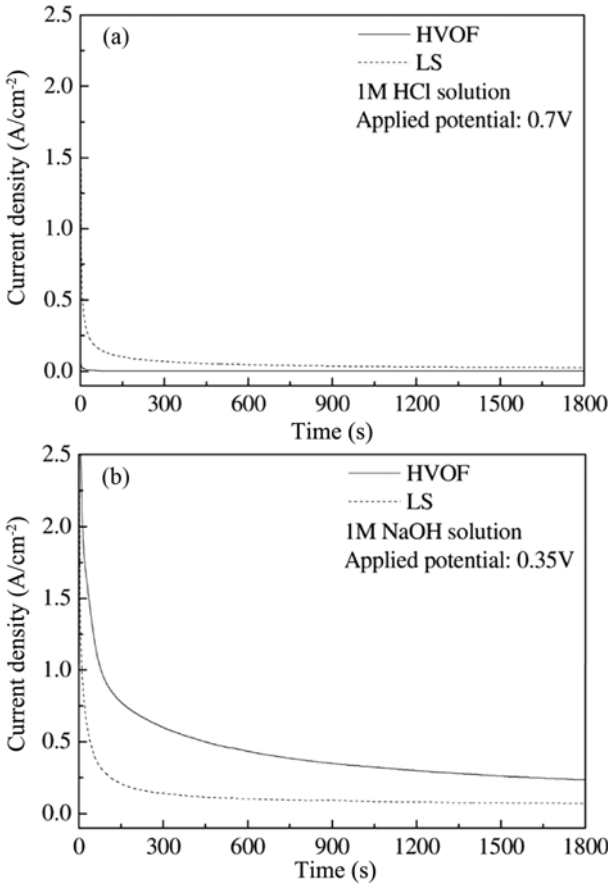

Fig. 7. Potentiostatic polarization curves of HVOF and LS coating in various solutions: (a) 1M HCl, (b) 1M NaOH.

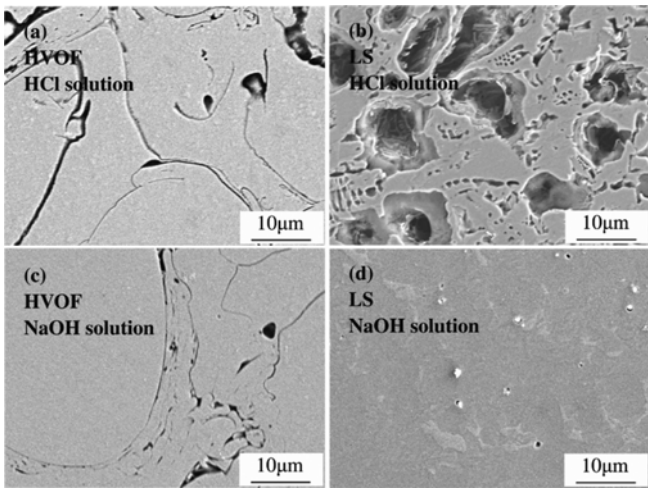

Fig. 8. Surface morphologies of (a), (c) HVOF coating and (b), (d) LS coating immersed in 1M HCl and NaOH solution, respectively.

were selected from the potentiodynamic polarization curves. The current densities decreased continuously with time and subsequently reached a steady state. Such smooth shapes of the curves indicate that a stable layer formed on the surface during the entire measurement period. The SEM surface images after the potentiostatic polarization measurement are shown in Fig. 8. The surfaces of the HVOF coating corroded in the HCl and the NaOH solution exhibit uniform surface microstructures, as shown in Fig. 8a and c, respectively. On the surface of the LS coating, a thick and porous layer can be observed after the test in the HCl solution, as shown in Fig. 8(b). After the test in the NaOH solution, however, the surface of the LS coating is covered by a uniform passive film, as shown in Fig. 8d.

4. DISCUSSION

The corrosion test results indicate that the HVOF coating holds higher corrosion resistance than the LS coating in acidic solution. It should be noted that the metallic glass is homogeneous in composition and microstructure without crystalline defects such as a grain boundary, precipitates or segregations where corrosion can occur preferentially. The surface homogeneity reduces the tendency of the formation of corrosion micro-cells and facilitates the formation of structurally homogeneous stable passive films. In the HCl solution, a stable passive film mainly composed of chromium oxides, iron oxides and some oxyhydroxides can be formed on the surface, inhibiting the dissolution of alloying elements from the surface [16,17]. However, since the LS coating layer includes different phases, sites with different corrosion susceptibility can be formed in the acidic solution and thus, the dissolution of the phase with low corrosion resistance can be facilitated by a galvanic coupling [18]. Moreover, relatively small chloride ions can diffuse quickly through crystalline defects, causing pitting and crevice corrosion, as shown in Fig. 8(b) [19,20].

In the NaOH solution, firstly, Fe in the anodic electrode will be dissolved following the reaction (2) [21,22]:

$$Fe + 2H_2O = Fe(OH)_2 = 2H^+ + 2e \quad (2)$$

Therefore, the $Fe(OH)_2$ is easily precipitated on the surface of the electrode. As the reaction proceeds, most of the $Fe(OH)_2$ will be continuously oxidized to FeOOH and Fe_2O_3 [23,24], which are thermodynamically stable in the alkaline solution. Moreover, the outward diffusion of Fe ions is faster than those of other metallic ions and thus, a large amount of iron oxides can continuously precipitate on the outermost surface resulting in a uniform passive film, as shown in Fig. 8c or d. Generally, for the same composition, the corrosion resistance of the coating is improved by lower porosity or higher amorphous phase content [25,26]. In this study, though the HVOF coating was an amorphous structure, the existence of a great number of pores may be attributed to the slightly lower corrosion resistance of the HVOF coating versus the LS coating in NaOH solution.

5. CONCLUSIONS

Coatings with the nominal composition of $Fe_{68.5}C_{7.1}Si_{3.3}B_{5.5}P_{8.7}Cr_{2.3}Mo_{2.5}Al_{2.0}$ were fabricated by HVOF and LS methods, respectively. An amorphous coating layer was formed by the HVOF method, while a coating layer with a crystalline dendritic microstructure involving various borides and carbides were formed by the LS method. The HVOF coating exhibited excellent corrosion resistance, since a uniform and stable film can be formed in the acidic solution. In the alkaline solutions, the HVOF coating with higher porosity exhibited slightly lower corrosion resistance than the LS coating. The excellent corrosion resistance of the amorphous coating prepared by the commercial HVOF method using Fe-BMG powders demonstrates the viability of Fe-BMG as a potential coating material for extensive practical anti-corrosive applications.

ACKNOWLEDGMENTS

The work was supported by the Korean Ministry of Commerce, Industry and Energy under the project for the development of structural metallic materials and parts with super strength and high performance. Also, financial support from RIST is deeply appreciated.

REFERENCE

1. S. J. Pang, T. Zhang, K. Asami, and A. Inoue, *Acta Materialia* **50**, 489 (2002).

2. A. Inoue, B. L. Shen, and C. T. Chang, *Intermetallics* **14**, 936 (2006).
3. K.-B. Lee, K.-W. Park, S.-H. Yi, and J.-C. Lee, *Korean J. Met. Mater.* **48**, 1 (2010).
4. A. Basu, A. N. Samant, and S. P. Harimkar, *Surf. Coat. Tech*. **202**, 2623 (2008).
5. H. W. Jin, Y. M. Rhyim, and M. C. Kim, *Met. Mater. Int*. **3**, 60 (1997).
6. Z. L. Long, Y. Shao, and A. Inoue, *Intermetallics* **15**, 1453 (2007).
7. S. J. Pang, T. Zhang, and A. Inoue, *Corros. Sci*. **44**, 1847 (2002).
8. V. Ponnambalam and S. J. Poon, *J. Mater. Res*. **19**, 1320 (2004).
9. Z. M. Wang, Y. T. Ma, and J. Q. Wang, *Electrochim. Acta*. **54**, 261 (2008).
10. H. X. Li, S. H. Yi, and H. S. Sohn, *J. Mater. Res*. **22**, 164 (2007).
11. H. X. Li, Z. P. Lu, and S. H. Yi, *Met. Mater. Int*. **15**, 7 (2009).
12. A. Inous, B. L. Shen, and C. T. Chang, *Acta Mater.* **52**, 4093 (2004).
13. D. C. Qiao, B. Green, and M. Morrison, *Rev. Adv. Mater. Sci*. **18**, 149 (2008).
14. Z. L. Long, C. T. Chang, and A. Inoue, *J. Non-Cryst. Solids* **354**, 4609 (2008).
15. M. G. Fontana, *Corrosion Engineering, 3^{ed}*., p.197, McGraw-Hill, New York (1986).
16. X. Y. Li, E. Akiyama, and K. Hashimoto, *Corros. Sci*. **41**, 1849 (1999).
17. M. F. Lopez, M. L. Escudero, and E. Vida, *Electrochim. Acta*. **42**, 659 (1997).
18. C. A. C. Souza, J. E. May, and C. S. Kiminami, *J. Non-Cryst. Solids* **284**, 99 (2001).
19. J. M. Guilemany, N. Cinca, and S. Dosta, *Corros. Sci*. **51**, 171 (2009).
20. Y. Ma, Y. Li, and F. H. Wang, *Corros. Sci*. **51**, 997 (2009).
21. G. H. Kelsall and R. A. Williams, *J. Electrochem. Soc*. **138**, 931 (1991).
22. C. Remazeilles and P. Refait, *Corros. Sci*. **50**, 856 (2008).
23. J. Pena, E. Torres, and M. J. Turrero, *Corros. Sci*. **50**, 2197 (2008).
24. A. J. Salkind and C. J. Venuto, *J. Electrochem. Soc*. **111**, 493 (1964).
25. A. P. Wang, X. C. Chang, W. L. Hou, *Mater. Sci. Eng. A* **449-451**, 277 (2007).
26. Z. Zhou, L. Wang, and F. C. Wang, *Surf. Coat. Tech*. **204**, 563 (2009).